

Supporting Information for “Ionospheric Conductances Derived From Electrodynamic Models”

D. R. Weimer^{1,2} and Thom R. Edwards³

¹Center for Space Science and Engineering Research, Virginia Tech, Blacksburg, Virginia, USA

²National Institute of Aerospace, Hampton, Virginia, USA

³Danish Technical University, Copenhagen, Denmark

Contents of this file

1. Figures S1 to S13

Introduction

This Supporting Information contains 13 additional figures that supplement the figures included in the main body of the paper. Figures S1–S4 show input values and conductivity results for dipole tilt angles of -23° and $+23^\circ$ for the Interplanetary Magnetic Field (IMF) clock angles of 90° and 270° , with an IMF magnitude of 10 nT. Figures S5–S13 show the same maps but for an IMF magnitude of 5 nT, for three dipole tilt angles (-23° , 0° , $+23^\circ$) at three IMF clock angles (90° , 180° , 270°). In all figures the solar wind velocity is 450 km/s and the $F_{10.7}$ index is 160 sfu. The format is the same as Figures 4–8 in the paper:

In the top row of each figure, maps (a)-(c) shows the electric potential and the two horizontal components of the electric field. The longitudes are marked in Magnetic Local Time (MLT), in magnetic apex coordinates, with the sun at 12 noon. The gray area on the maps show the region that is outside of the cap that is used in the SCHA functions in the model. Minimum and maximum values of the potential and electric fields are indicated in the lower left and right corners of all contour maps, and the locations where these values are found are marked on the map with the diamond and plus symbols respectively.

In the second row of these figures, maps (d)-(f) show the equivalent current function and the duskward and sunward components of the divergence-free currents that are calculated from the gradients of this function. The color bar scale for all horizontal currents is adjusted to approximately match the largest magnitude of the sunward current.

In the third row, map (g) shows the field-aligned current (FAC) and (h)-(i) show the duskward and sunward components of the curl-free current. Lines are drawn only for every third interval marked on the color bar to reduce crowding around the peaks. The gray area on the maps show the region outside of the boundaries of the FAC model. The total sums of the upward (negative) and downward (positive) FAC, integrated over the spherical cap, are indicated in the upper left and right corners of the contour map in units of millions of Amperes (MA).

The fourth row starts with the Poynting flux, (j), calculated from the cross product of the electric and magnetic fields. The total energy flow into the ionosphere is in the upper-right corner, in Giga-watts (GW). The second map in the fourth row, (k), shows the Pedersen conductivity that is calculated without use of the divergence-free component

of the horizontal current. Map (l) shows the Hall conductivity that is calculated without use of the curl-free current.

The map at the left in the bottom row, (m) shows the Joule heating that is calculated with from the dot product of the electric field and the total current. Maps (n) and (o) in the bottom row show the final values of the Pedersen conductivity and Hall conductivities, derived using the total currents.

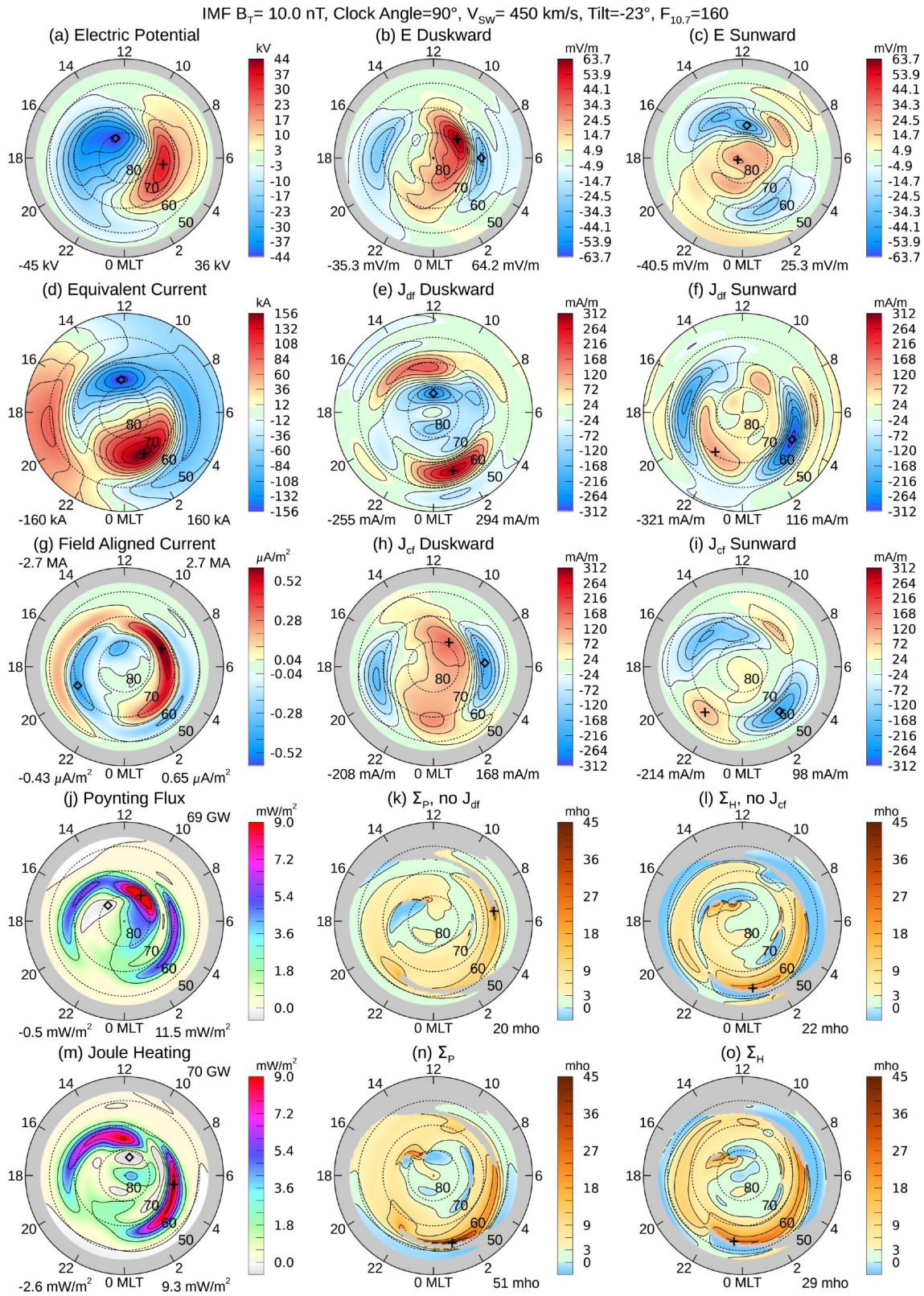


Figure S1. Conductivity input data and results, for IMF B_T magnitude 10 nT at 90° clock angle, and the dipole tilt angle is -23° .

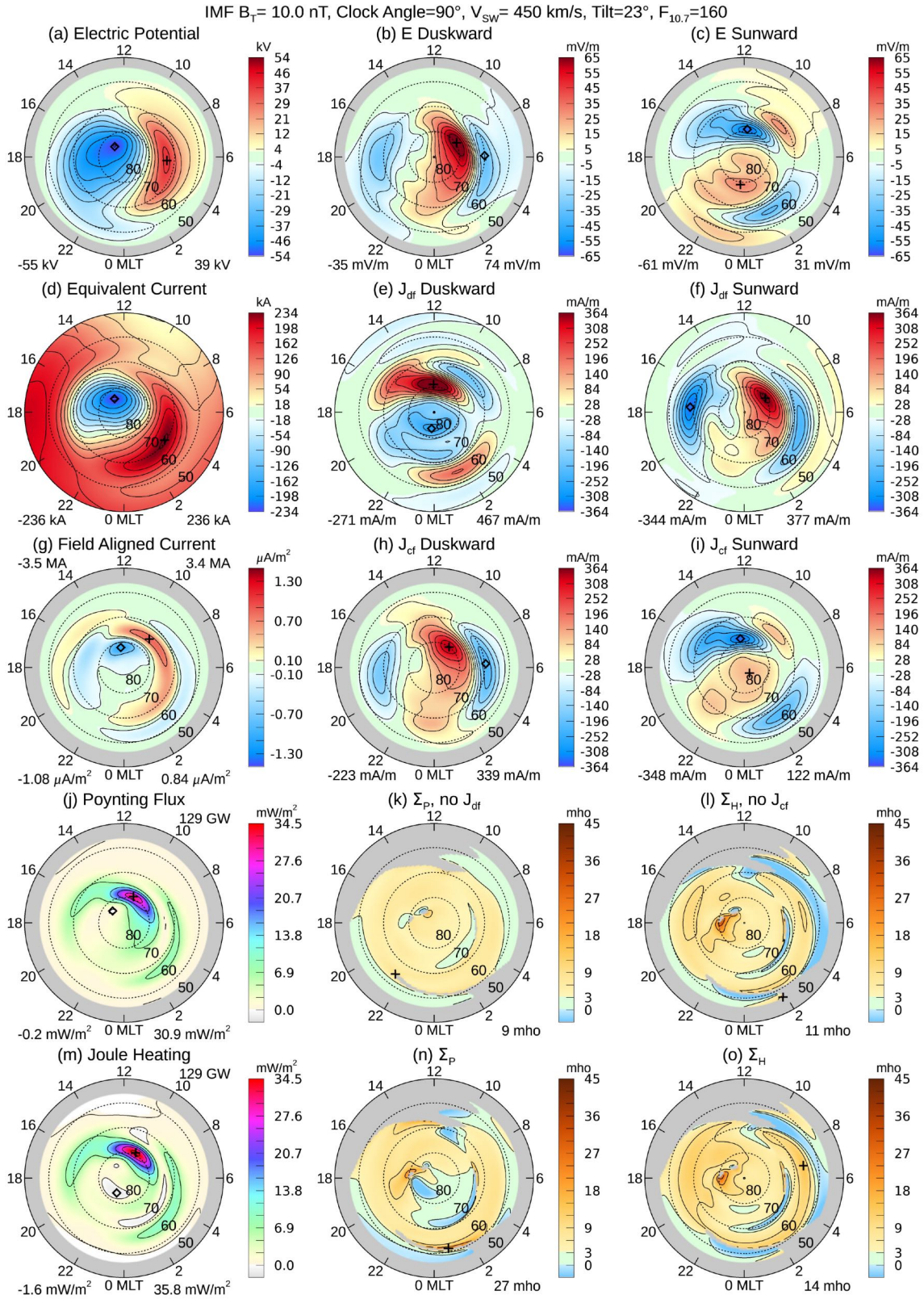


Figure S2. Conductivity input data and results, for IMF B_T magnitude 10 nT at 90° clock angle, and the dipole tilt angle is $+23^\circ$.

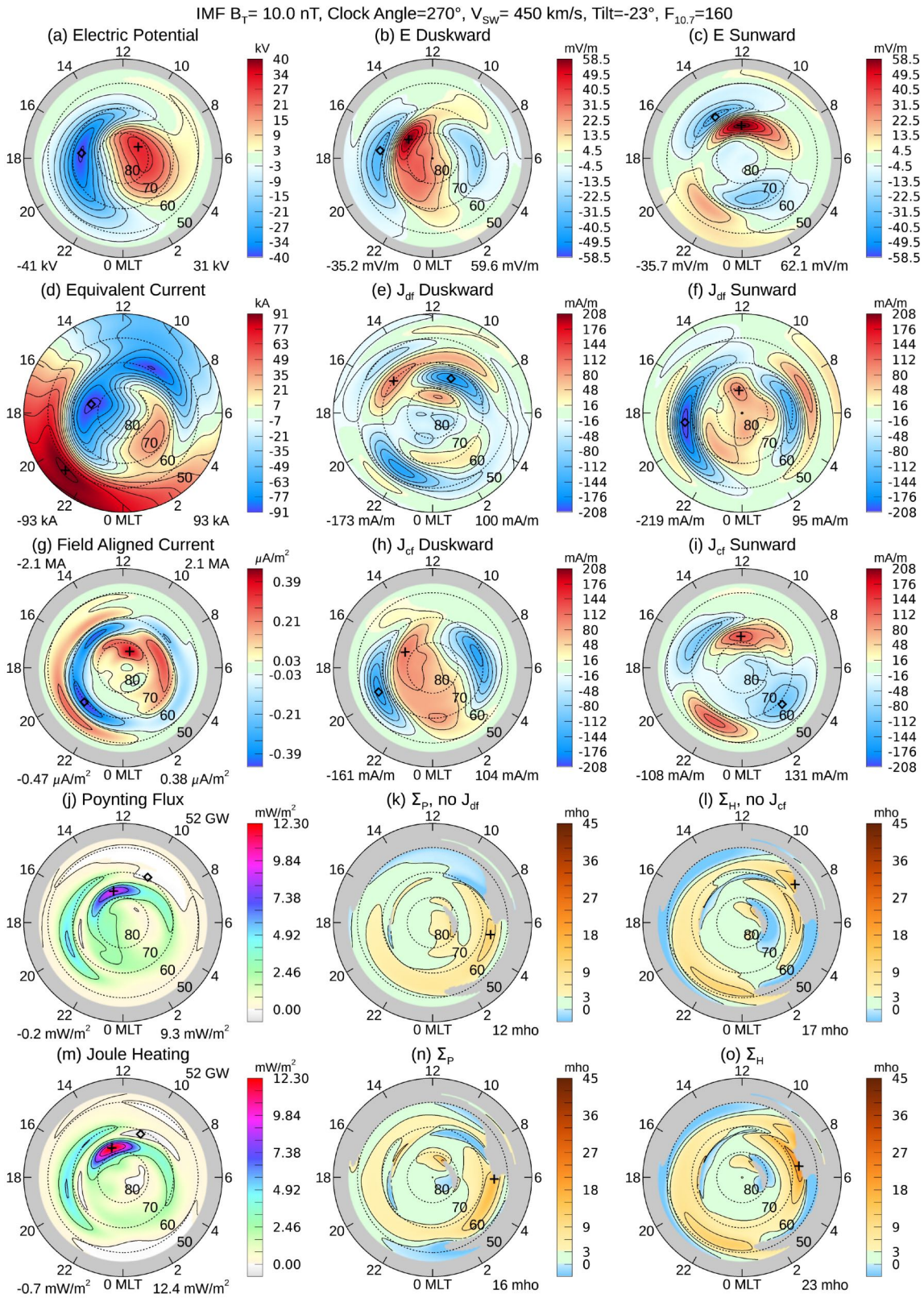


Figure S3. Conductivity input data and results, for IMF B_T magnitude 10 nT at 270° clock angle, and the dipole tilt angle is -23° .

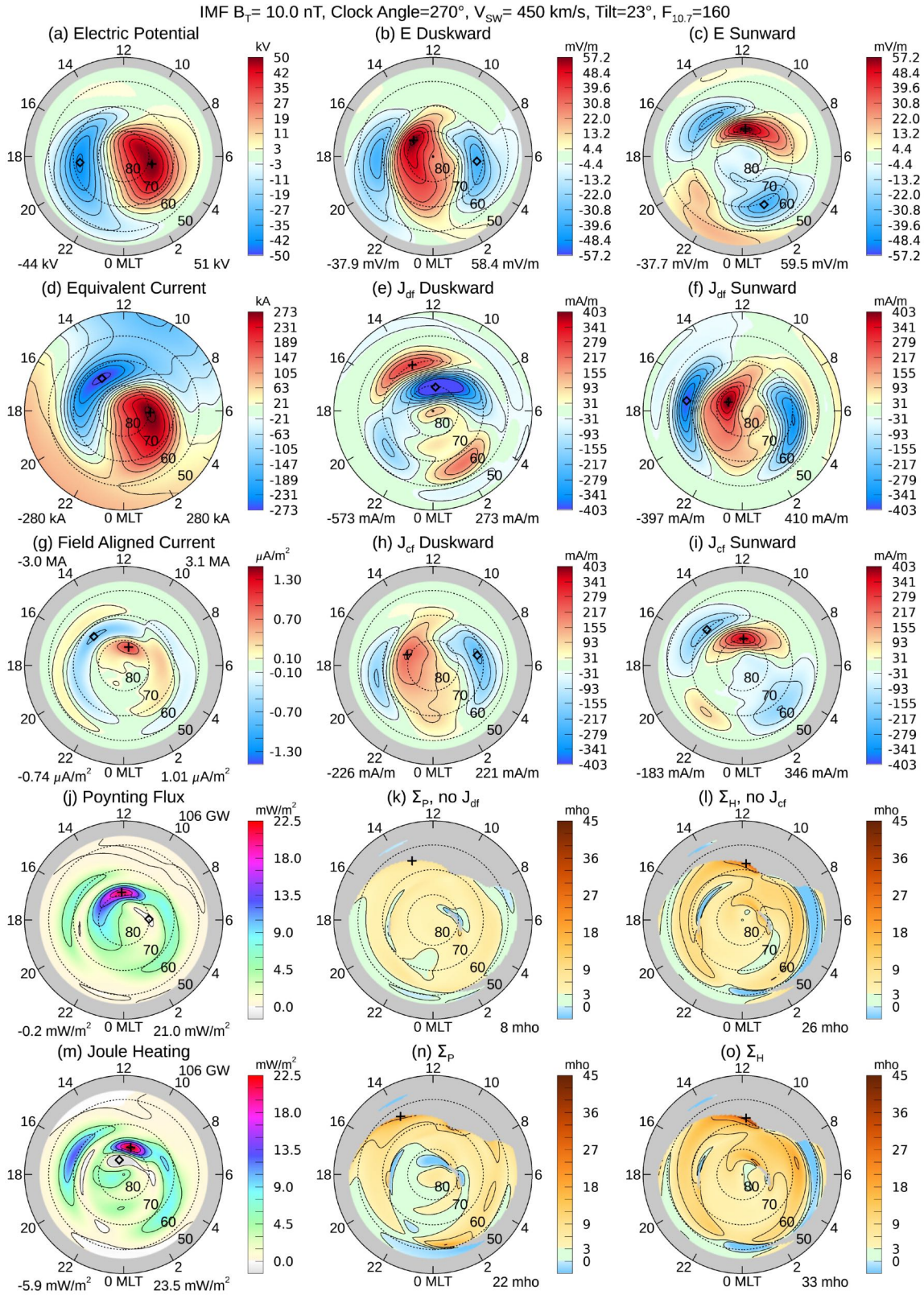


Figure S4. Conductivity input data and results, for IMF B_T magnitude 10 nT at 270° clock angle, and the dipole tilt angle is $+23^\circ$.

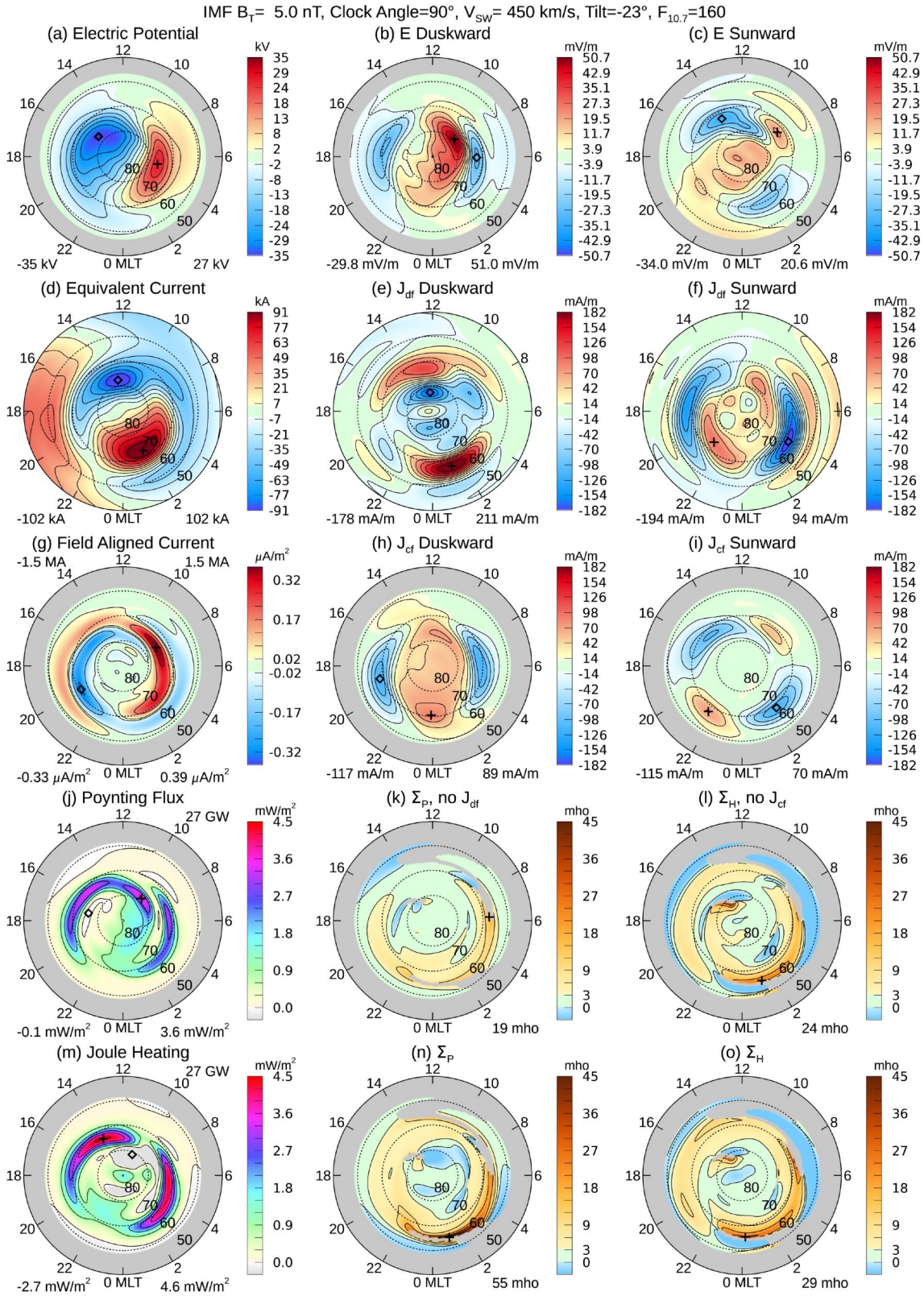


Figure S5. Conductivity input data and results, for IMF B_T magnitude 5 nT at 90° clock angle, and the dipole tilt angle is -23° .

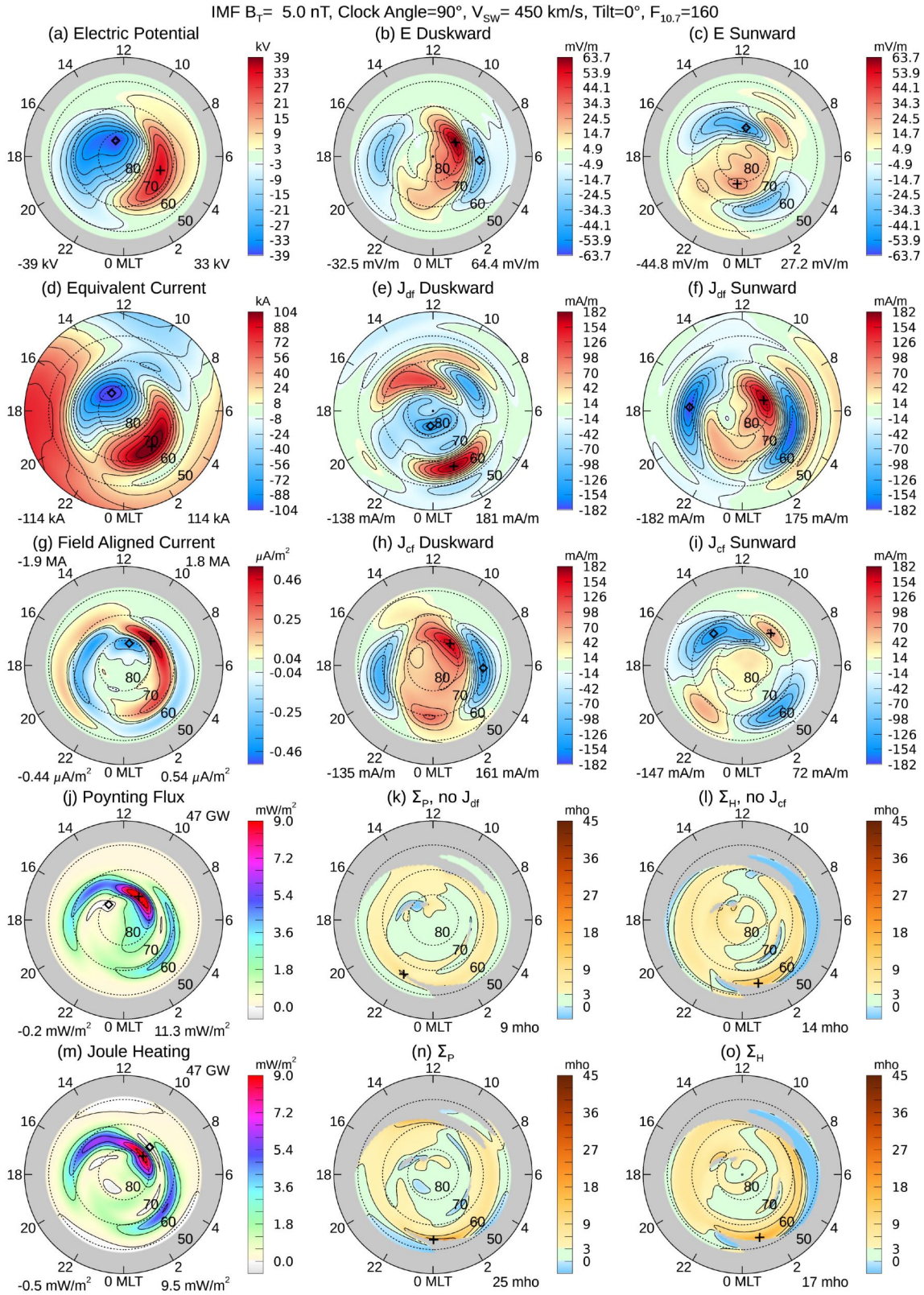


Figure S6. Conductivity input data and results, for IMF B_T magnitude 5 nT at 90° clock angle, and the dipole tilt angle is 0° .

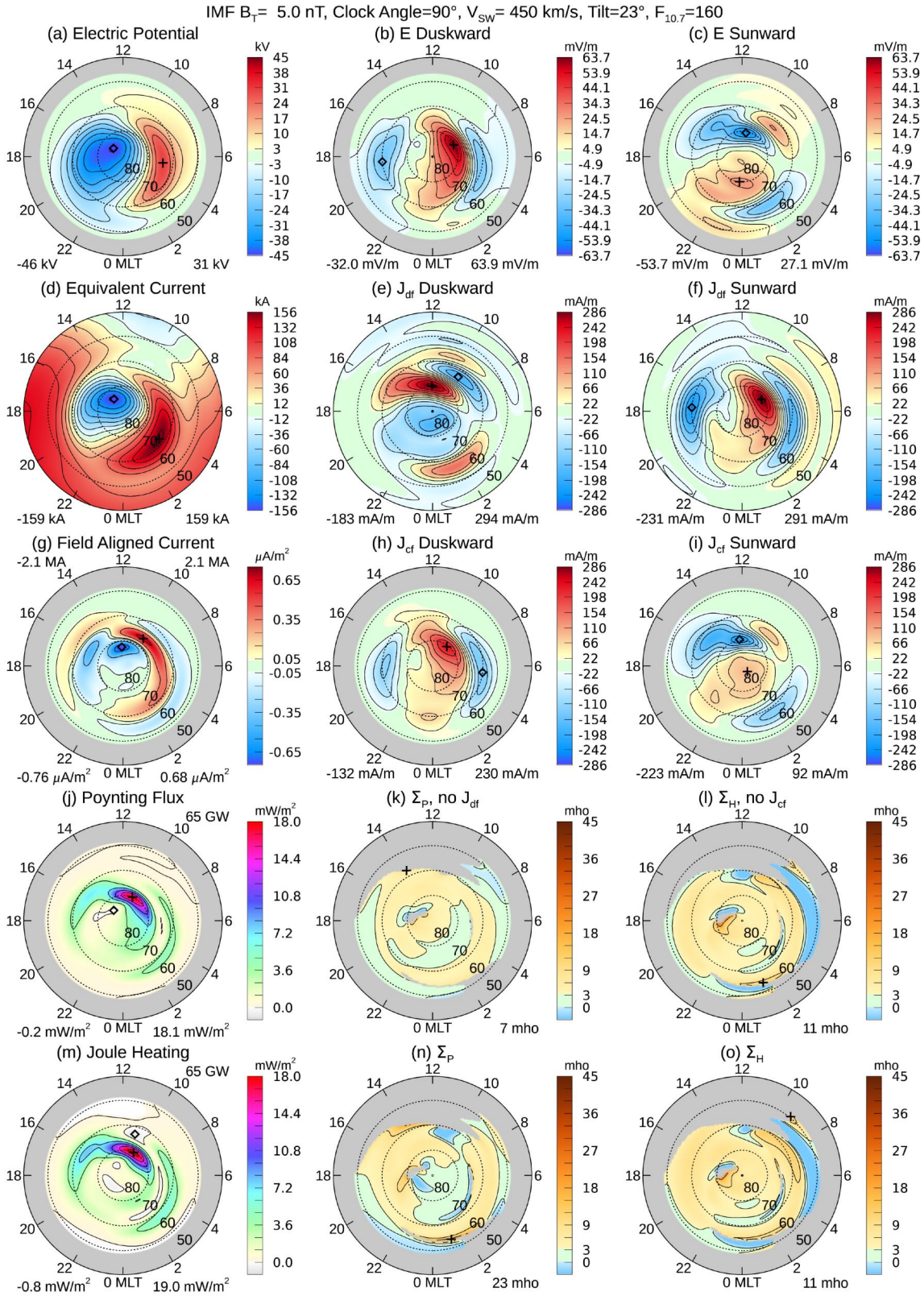


Figure S7. Conductivity input data and results, for IMF B_T magnitude 5 nT at 90° clock angle, and the dipole tilt angle is $+23^\circ$.

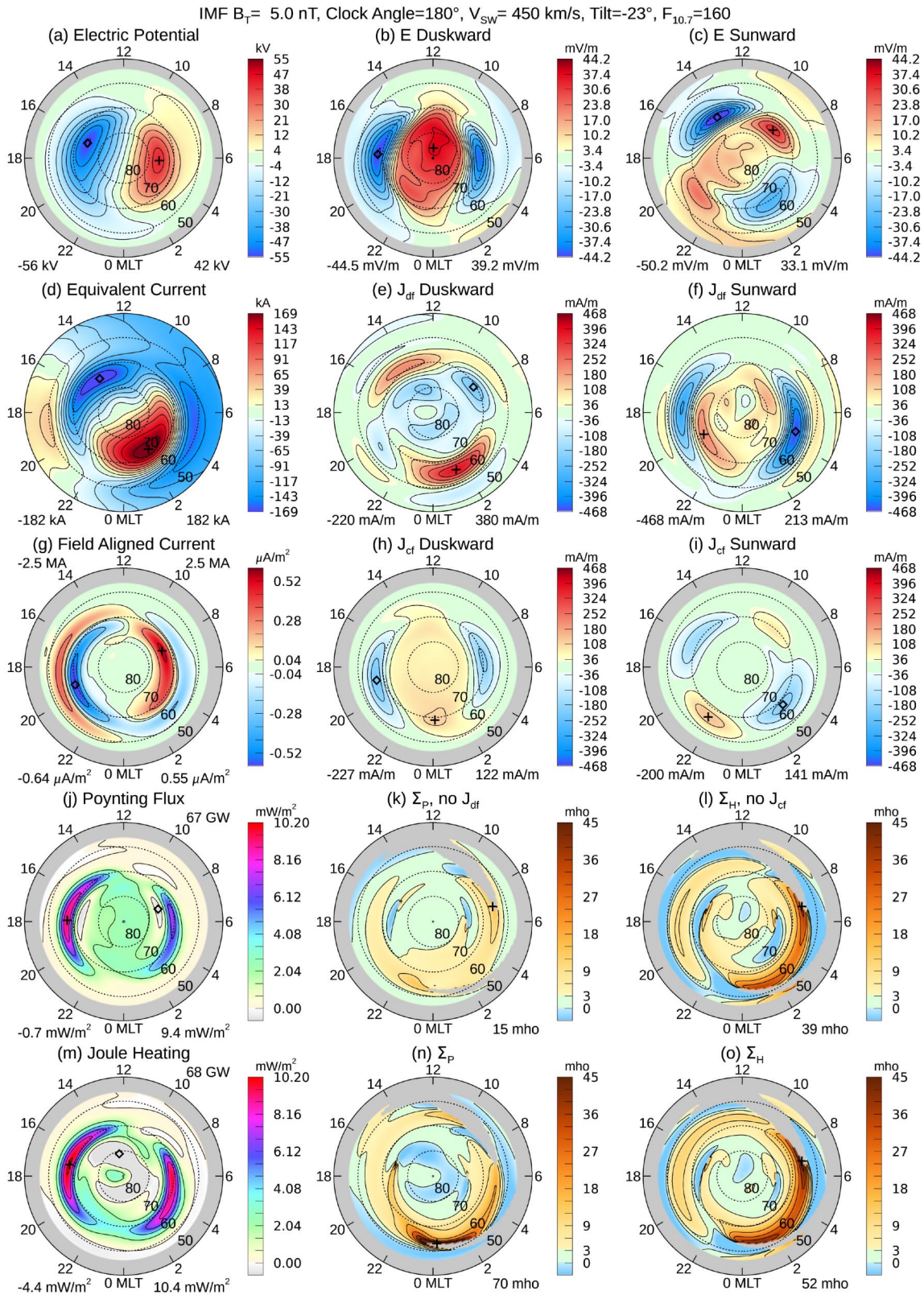


Figure S8. Conductivity input data and results, for IMF B_T magnitude 5 nT at 180° clock angle, and the dipole tilt angle is -23° .

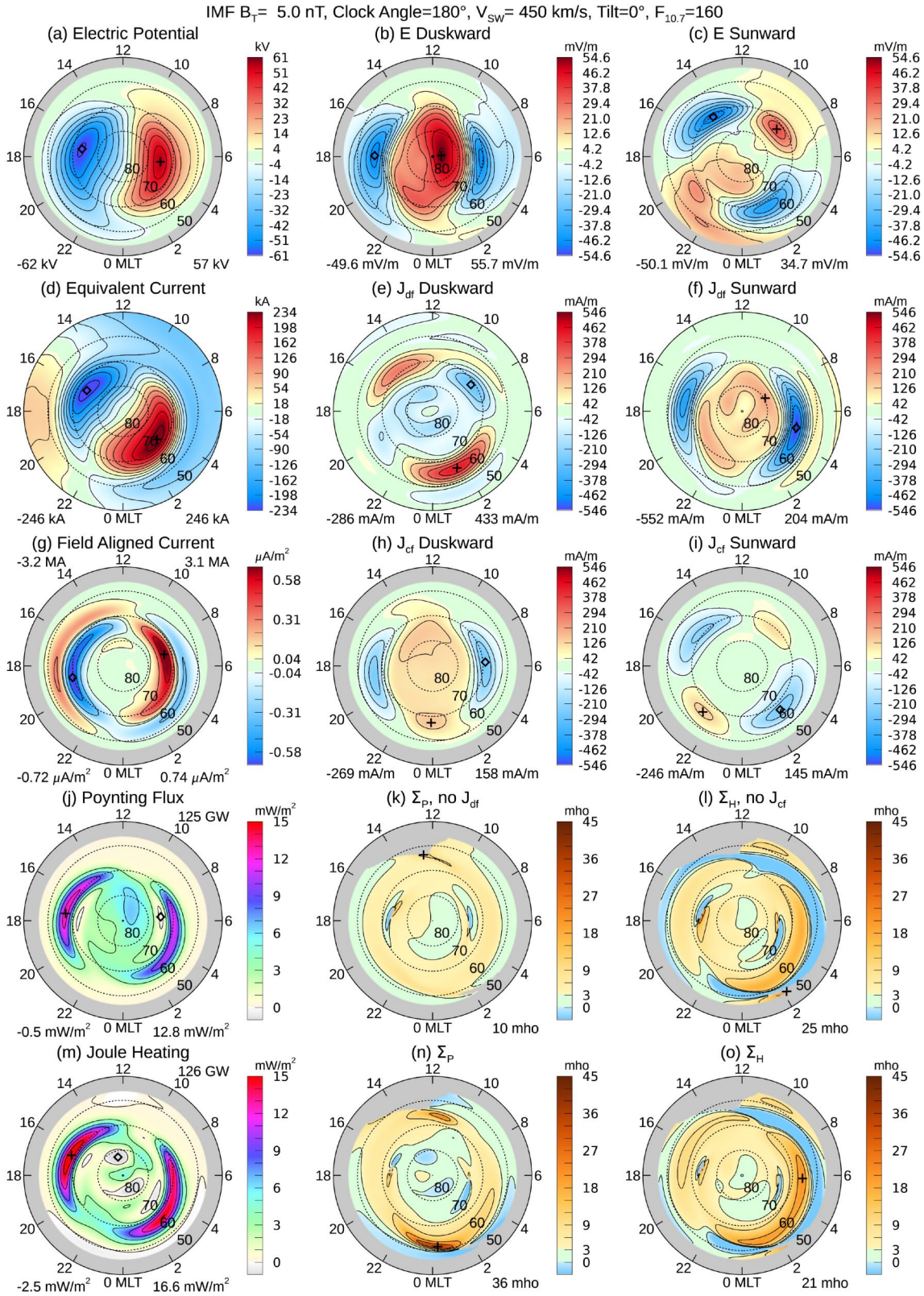


Figure S9. Conductivity input data and results, for IMF B_T magnitude 5 nT at 180° clock angle, and the dipole tilt angle is 0° .

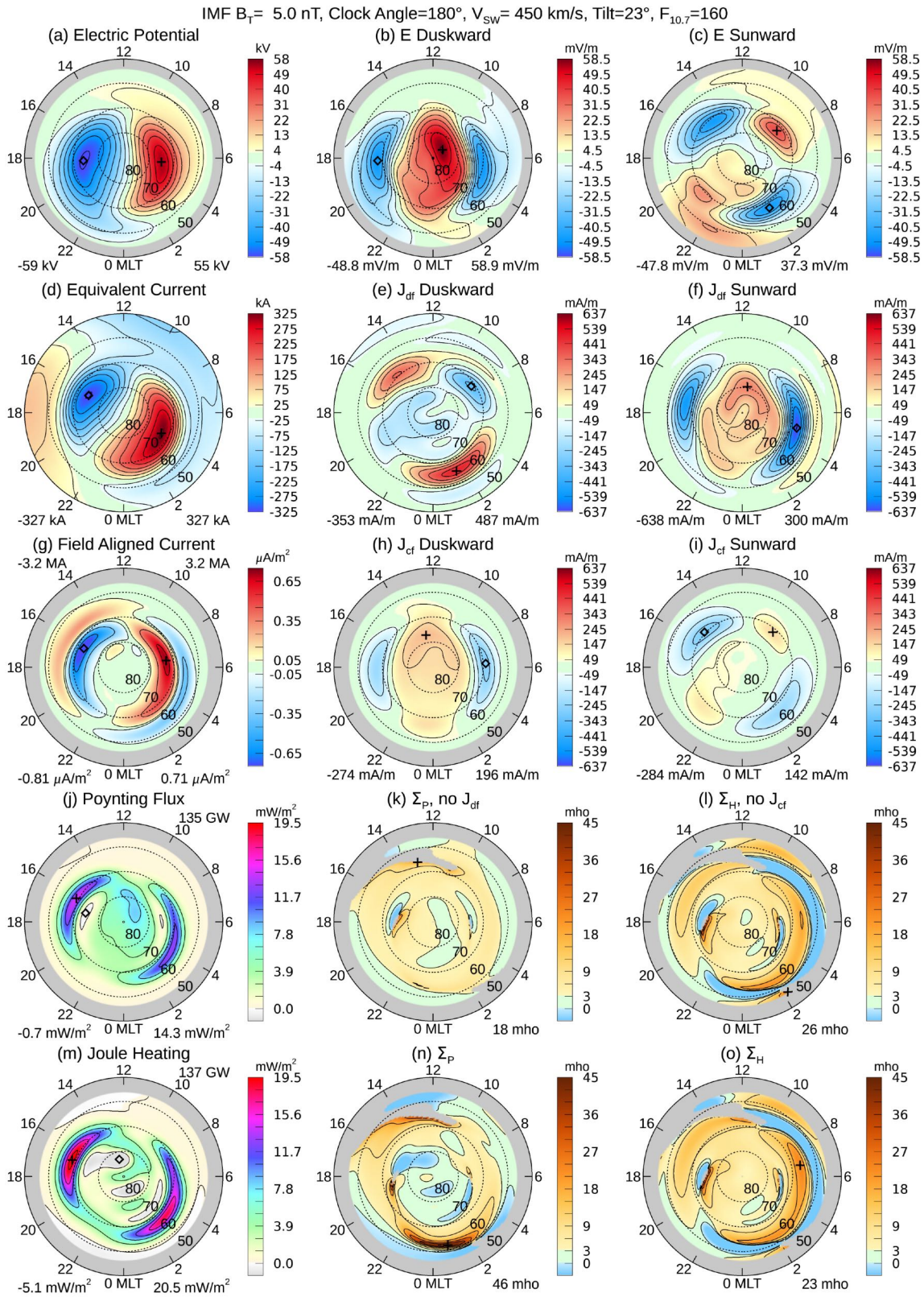


Figure S10. Conductivity input data and results, for IMF B_T magnitude 5 nT at 180° clock angle, and the dipole tilt angle is $+23^\circ$.

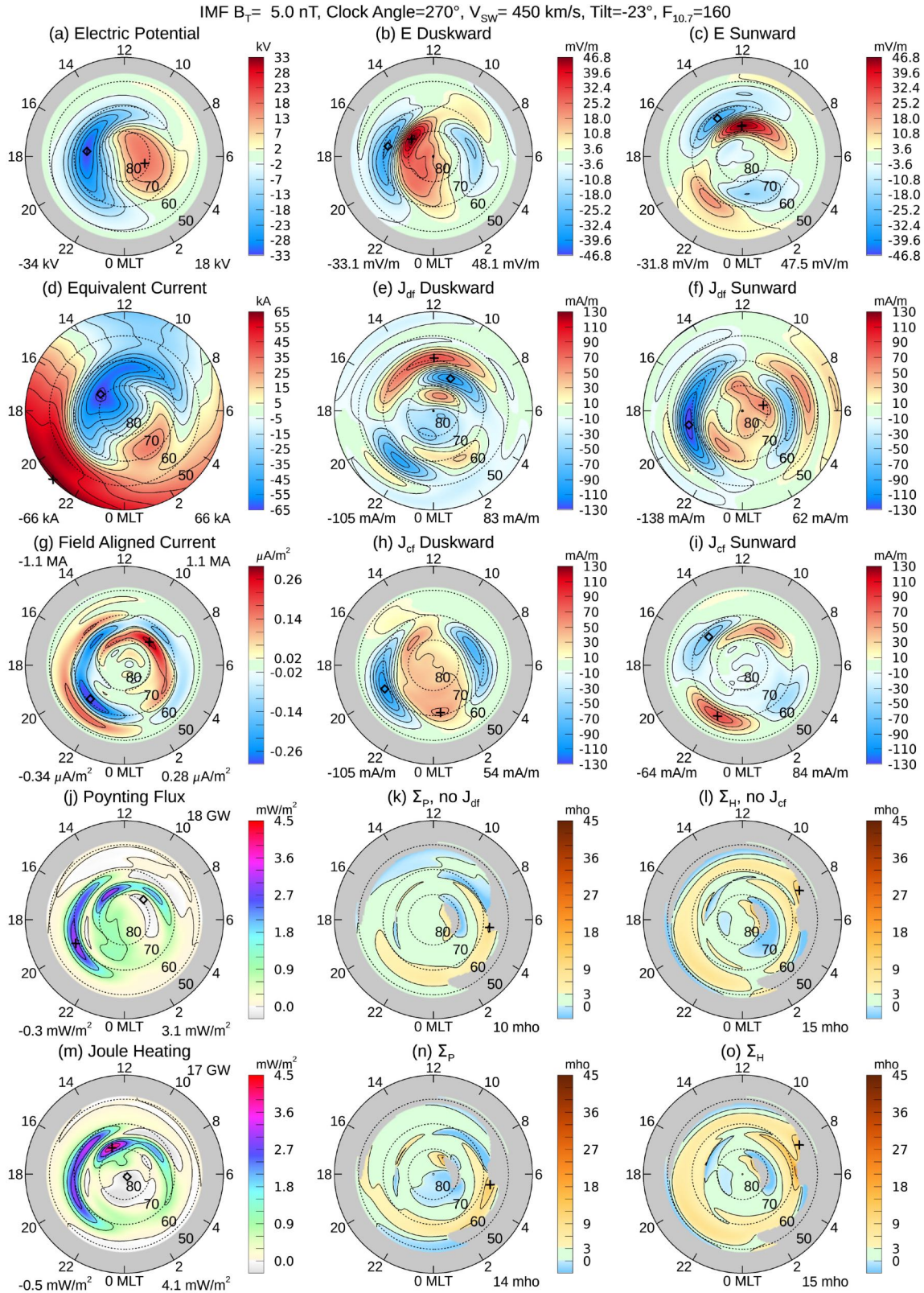


Figure S11. Conductivity input data and results, for IMF B_T magnitude 5 nT at 270° clock angle, and the dipole tilt angle is -23° .

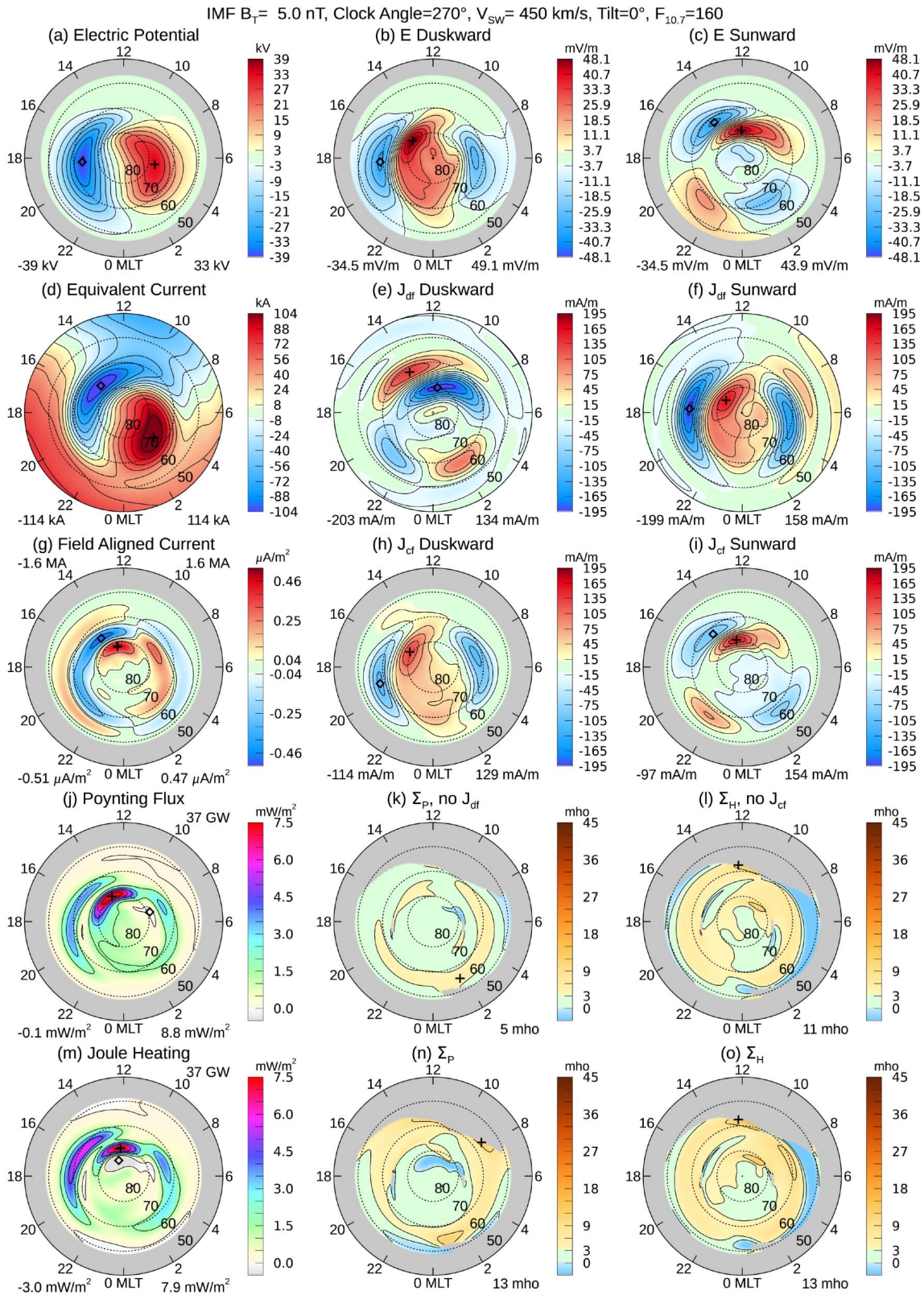


Figure S12. Conductivity input data and results, for IMF B_T magnitude 5 nT at 270° clock angle, and the dipole tilt angle is 0° .

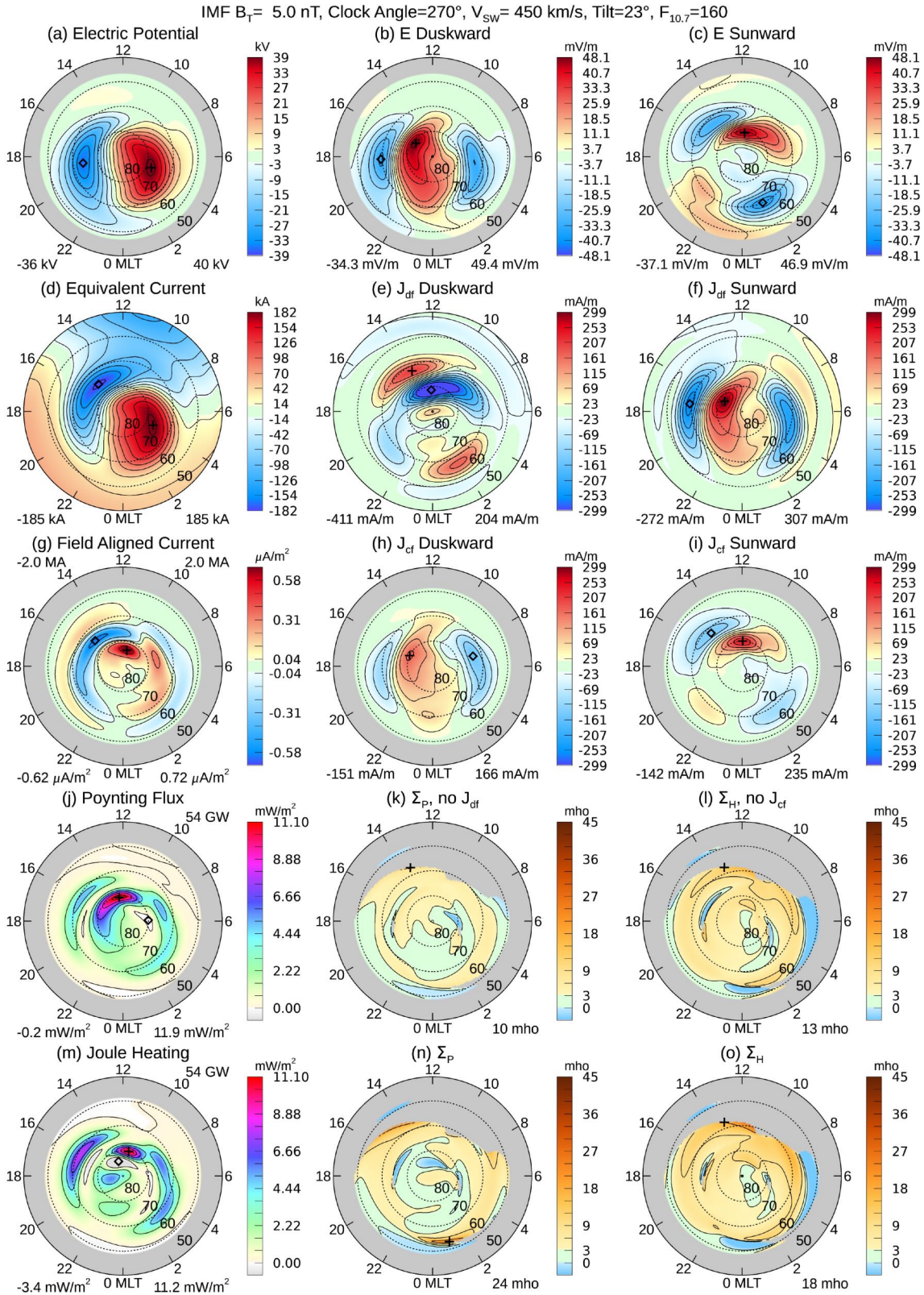


Figure S13. Conductivity input data and results, for IMF B_T magnitude 5 nT at 270° clock angle, and the dipole tilt angle is $+23^\circ$.